DCB 2023

II Младежка научна конференция с международно участие
„Проектиране и строителство на сгради и съоръжения“, 09-10 ноември 2023г., София

II Youth Scientific Conference with international participation
„Design and Construction of Buildings and Facilities“, November 09-10, 2023, Sofia, Bulgaria
ISSN 2738-7887 (online); ISSN 2738-7879 (CD-ROM)

THE EDITORS WILL TRANSLATE THE TITLE FROM THE ENGLISH VERSIONS

ПАРАМЕТРИЧНО ИЗСЛЕДВАНЕ НА ОГЪВАЩ МОМЕНТ В НАПУКАНА СТОМАНОБЕТОННА ГРЕДА

Емре Юсуф[1], Ирина Керелезова[2]

PARAMETRIC STUDY OF THE BENDING MOMENT IN A CRACKED RC BEAM

Yusuf Emre[1], Kerelezova Irina[2]

Abstract:
In this paper we present the results of an initial parametric study of the maximum moment in a simple beam loaded in bending. The investigated RC beam is three-point loaded with a rectangular cross-section. The area of the main flexural crack is modelled with fracture mechanics methods, allowing for crack propagation. Multiple numerical solutions were performed varying the reinforcement ratio, steel type and concrete strength. The aim is to investigate the maximum moment dependence on the present parameters in the assumed model. This analysis is the preliminary stage of a project to determine the maximum bending moment in a reinforced concrete beam in bending considering the concrete tensile strength.

Keywords:
Cracked RC beam, bending moment, fracture mechanics.

1. INTRODUCTION

In the calculation of the reinforced concrete beams subjected to bending, it is assumed that yield strength is reached in the reinforcement, and the compressive strength of the concrete is reached in the compressive zone. Considering these assumptions, the work of the concrete in tension as well as the crack growth resistance are completely excluded. As a result, a simplified practical formula for calculating the maximum bending moment is obtained, which does not consider the significant effects of the concrete's performance. In the present work, a beam in bending with a single-reinforced section is considered, and a nonlinear numerical model considering these effects is used to determine the stresses in the concrete. The aim is to verify the variance of the results by a more realistic model of the concrete in the crack opening process. A parametric analysis by changing some variables, such as strength of concrete and reinforcement or reinforcement ratio, has been performed. Certain comparisons and conclusions have been made. Ideas for further work and research are outlined.

[1] Yusuf Emre, Student, Structural mechanics, Faculty of civil engineering, University of Architecture, Civil Engineering and Geodesy, E-mail: emre00yu@gmail.com

[2] Kerelezova Irina, PhD assoc. prof., Structural mechanics, Faculty of civil engineering, University of Architecture, Civil Engineering and Geodesy, E-mail: igk_fce@uacg.bg

2. NUMERICAL MODELLING

2.1. The beam model and theory

In the present work, a model working with Hillerborg's theory of concrete [1] is used for modelling the fracture process zone. Figure 1 represents the main idea of this theory.

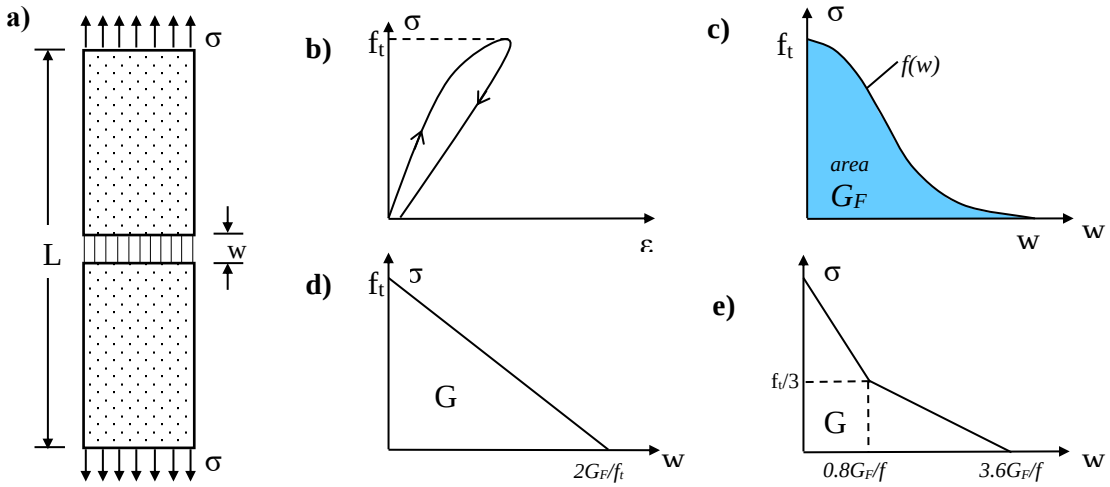

Figure 1. Hillerborg’s theory (a) concrete element on tension, (b) ($\sigma - \varepsilon$) diagram out of the fracture zone, (c) ($\sigma - w$) diagram in the fracture zone (d) and (e) numerical modelling of the ($\sigma - w$) diagram.

According to the Hillerborg’s theory the development of the fracture (or process) zone is introduced by a “fictitious” crack and is shown in Figure 1.a, where the stress-deformation behavior is investigated in a deformation controlled uniaxial tension test. As load increase the stresses are increasing almost linearly up to their ultimate tensile capacity. That point corresponds to the tensile strength f_t of the concrete (see Figure 1.b)). At this stage microcracks are developed. Further loading will result in a descending branch, called “softening in tension”. As the stress decreases the parts outside the fracture zone are unloaded and that part of the body volume remains elastic. The fracture is concentrated in the local zone where it is started. In the fracture zone the behavior is presented by stress-relative displacement curve ($\sigma - w$) – fig. 1 c).

In the displayed model in the fracture process zone nonlinear springs represent the concrete’s behavior. For spring’s law the relationship from fig. 1 d) has been used. Figure 2 shows the basic idea of the Combin39 spring finite element in ANSYS [5].

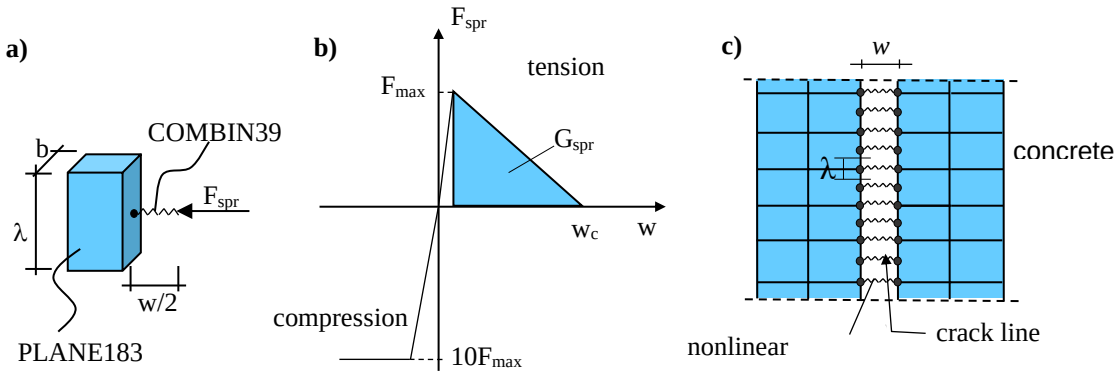

Figure 2. Nonlinear springs (a) spring’s zone, (b) linear spring model, (c) FE model.

In the provided model, the reinforcement bars are also modelled as a spring element, but with the physical characteristics of steel.

In theoretical formulation, it is necessary to know the fracture energy value, which is a material constant. For this investigation, the fracture energy is assumed to be G_f = 0,124 which is an average value for concrete.

The model of the analyzed beam is taken from the work of Smarzewski and Słowik [2]. In this paper, experimental and numerical results for a three-point bending beam are presented. The beams are tested to failure and the numerical results corroborate with the experiment. As an initial stage, the authors of the present research have numerically modelled the concrete beams from the work of Smarzewski and Słowik with the theoretical formulation presented here, in order to validate the performance of the numerical model. After carrying out the control test solution, the actual work, namely parametric research, was started.

2.2. Beam control test

The theoretical and numerical models presented here were used by Kerelezova in other scientific studies such as [3], [4]. However, before starting the actual study of the beam in the present work, a test solution was made based on the work of Smarzewski and Słowik [2]. To verify the model, several solutions were performed, but due to the limited volume, the results for only one of them are included here. Geometry and physical characteristics are shown in fig. 3.

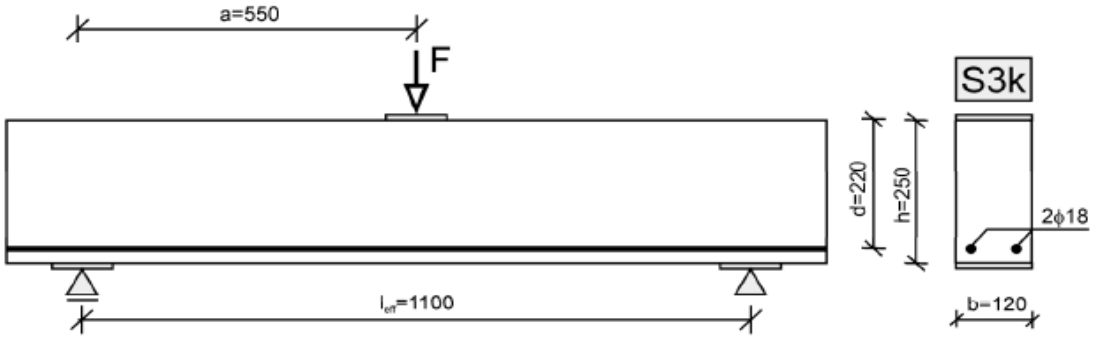

Beam	l_{eff} (m)	a/d	Longitudinal Reinforcement			
			Steel Bars	Reinforcement Ratio ρ (%)	Yield Stress f_y (MPa)	Tensile Strength f_t (MPa)
S3k	1.1	2.5	2ϕ18	1.8	453	698

Property	Number of Specimens	Mean Value (MPa)
Compressive strength, f_c	27	35.0
Tensile splitting strength, $f_{ct,sp}$	32	3.5
Young's modulus, E_c	19	41400

Figure 3. Test model of the beam.

The solution was performed using displacement control, because in the case of crack growth the force-controlled solution is not a converged. After performing a nonlinear solution in the ANSYS program [5], the force-displacement curve was plotted. The result of this solution together with the results of the work of Smarzewski and Słowik are presented in fig. 4.

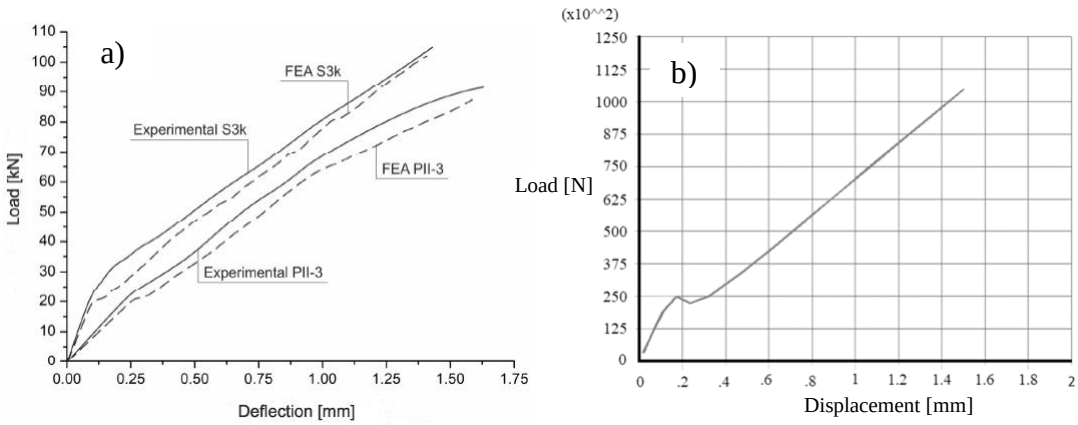

Figure 4. Load-displacement curves for test beam S3k: a) results from [2]; b) results from presented model.

As demonstrated on the graphs shown in figure 4, the results of the present model substantiate the experimental and numerical results of Smarzewski and Słowik's work. This gives the authors of the current study a reason to accept the presented numerical model as accurate and reliable enough to carry out further research.

2.3. Modelling of the parametric analysis beam

For the present study, as mentioned, the beam presented in the previous paragraph was used. The difference consists of a change in the physical characteristics of the concrete and a change of the reinforcement ratio. For this purpose, standard classes of concrete and steel were used in Eurocode 2 [6]. Table 1 presents the parameters that were varied and their combination.

Table 1. Parametrical combinations used in the analysis.

Concrete	Steel					Concrete	Steel				
C16/20	**B420**					**C30/37**	**B420**				
	2N10	2N12	2N14	2N16	2N18		2N10	2N12	2N14	2N16	2N18
	B500						**B500**				
	2N10	2N12	2N14	2N16	2N18		2N10	2N12	2N14	2N16	2N18
C20/25	**B420**					**C35/45**	**B420**				
	2N10	2N12	2N14	2N16	2N18		2N10	2N12	2N14	2N16	2N18
	B500						**B500**				
	2N10	2N12	2N14	2N16	2N18		2N10	2N12	2N14	2N16	2N18
C25/30	**B420**					**C40/50**	**B420**				
	2N10	2N12	2N14	2N16	2N18		2N10	2N12	2N14	2N16	2N18
	B500						**B500**				
	2N10	2N12	2N14	2N16	2N18		2N10	2N12	2N14	2N16	2N18

As shown in Table 1, for each class of concrete two types of steel are included as well as five variants of their reinforcement ratio. For each of these combinations, a nonlinear solution was performed with the model presented in the previous paragraph. The aim of this analysis is to investigate how the bending moment value changes at the maximum load capacity stage. For the same stage, the relative rotation at the maximum load stage is also considered.

2. NUMERICAL RESULTS

In this paragraph, the numerical results from the multiple nonlinear solutions performed are presented. For each nonlinear solution, the force-displacement curve was extracted. For the stage of the maximum value of the load, the stress distribution in the fracture zone is extracted. Taking this stress distribution and the reinforcement stress, the bending moment at maximum load stage was calculated. The relative rotation of the beam is also calculated. Figure 5 shows a typical stress diagram and force-displacement plot.

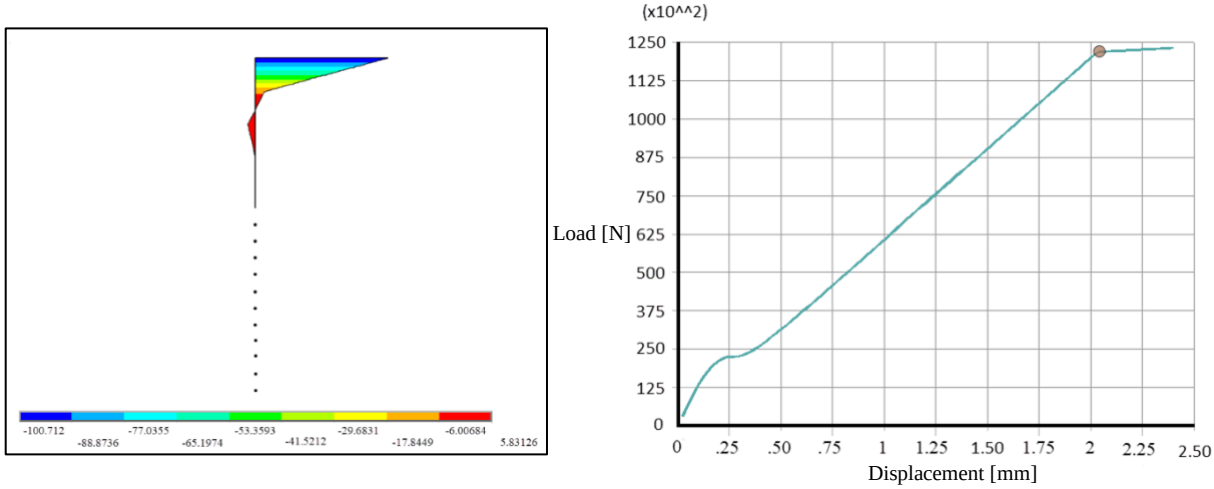

Figure 5. Typical normal stresses diagram in the process zone and the beam force-displacement curve.

The results shown in fig. 5 are for concrete class 16/20, steel type B420 and 2N10 reinforcement. As seen from the stress distribution at the maximum load stage, more than a half of the cross section is cracked with zero stresses. It is important to note that in the presented model the stresses in the compressive zone reach values greater than the concrete's strength, in other words, concrete plasticity is not taken into account. This has been done to facilitate the work on the parametric analysis research. As mentioned at the beginning of this article, this analysis is an initial stage of the investigation of the bending moment in a beam with consideration of the tensile strength of concrete. That is why at this primary stage the authors have chosen to exclude some parameters in the analysis.

Table 2 presents the results for the bending moment and the relative rotation from each of the solutions performed.

Table 2. Numerical results for the moment and the relative rotation.

		A_s [mm^2]	**2N10**	**2N12**	**2N14**	**2N16**	**2N18**
			157,08	226,19	307,88	402,12	508,94
		ρ	0,006	0,009	0,012	0,015	0,020
C16/20	B420	M [kNm]	**13,77**	**19,98**	**27,49**	**36,35**	**45,86**
		$\Delta\varphi$ [°]	0,1876	0,2668	0,3661	0,4759	0,6110
	B500	M [kNm]	**16,47**	**23,90**	**33,02**	**43,19**	**54,40**
		φ [°]	0,2216	0,3205	0,4377	0,5730	0,7429
C20/25	B420	M [kNm]	**13,77**	**20,05**	**27,36**	**36,17**	**46,02**
		$\Delta\varphi$ [°]	0,1846	0,2671	0,3591	0,4704	0,5947
	B500	M [kNm]	**16,46**	**23,91**	**32,82**	**43,30**	**54,55**
		$\Delta\varphi$ [°]	0,2185	0,3122	0,4299	0,5583	0,7134

		A_s [mm^2]	**2N10**	**2N12**	**2N14**	**2N16**	**2N18**
			157,08	226,19	307,88	402,12	508,94
		ρ	0,006	0,009	0,012	0,015	0,020
C25/30	B420	M [kNm]	**13,78**	**20,08**	**27,37**	**35,90**	**45,91**
		φ [°]	0,1822	0,2586	0,3508	0,4597	0,5856
	B500	M [kNm]	**16,50**	**23,93**	**32,65**	**43,09**	**54,75**
		$\Delta\varphi$ [°]	0,2155	0,3082	0,4197	0,5484	0,6972
C30/37	B420	M [kNm]	**13,77**	**20,12**	**27,47**	**35,91**	**45,72**
		$\Delta\varphi$ [°]	0,1747	0,2506	0,3400	0,4462	0,5890
	B500	M [kNm]	**16,55**	**24,02**	**32,67**	**42,90**	**54,66**
		$\Delta\varphi$ [°]	0,2096	0,3002	0,4195	0,5345	0,6771
C35/45	B420	M [kNm]	**13,74**	**20,12**	**27,51**	**35,98**	**45,56**
		$\Delta\varphi$ [°]	0,1722	0,2466	0,3345	0,4394	0,5586
	B500	M [kNm]	**16,56**	**24,08**	**32,79**	**42,84**	**54,53**
		$\Delta\varphi$ [°]	0,2066	0,2961	0,4002	0,5243	0,6667
C40/50	B420	M [kNm]	**13,84**	**20,13**	**27,59**	**36,04**	**45,62**
		$\Delta\varphi$ [°]	0,1724	0,2425	0,3319	0,4326	0,5496
	B500	M [kNm]	**16,55**	**24,07**	**32,85**	**42,91**	**54,38**
		$\Delta\varphi$ [°]	0,2037	0,2877	0,3954	0,5147	0,6564

Based on these results, graphs have been compiled giving a picture of the parametric dependencies for the bending moment and virtual rotation in the beam. Figures 6 and 7 show the relation of the bending moment and, respectively, the virtual rotation for the different classes of concrete for B420 steel. Figures 8 and 9 show the dependencies of the bending moment and, respectively, the relative rotation on the change of the concrete class for B500 steel.

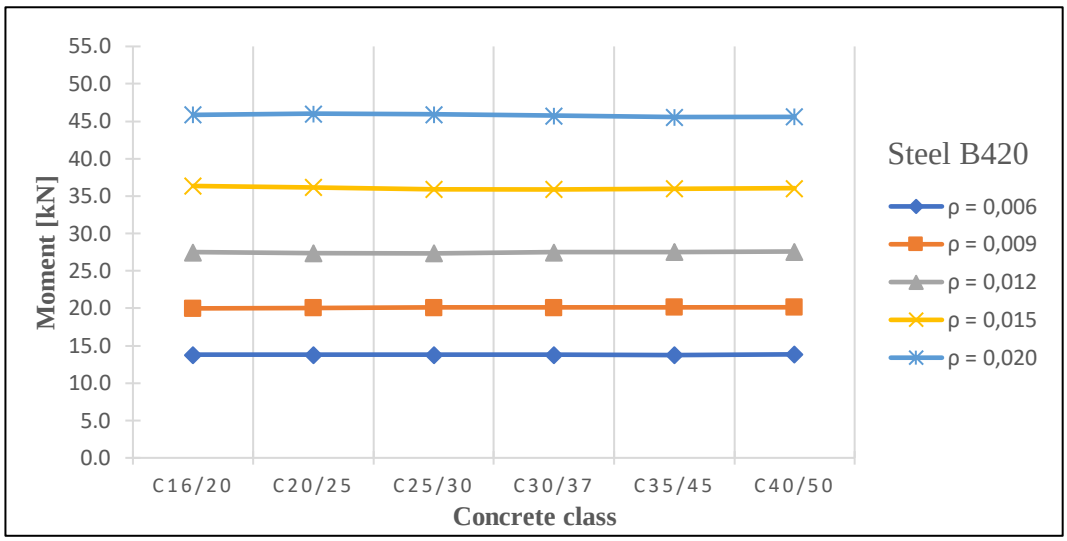

Figure 6. Bending moment-concrete class for steel B420.

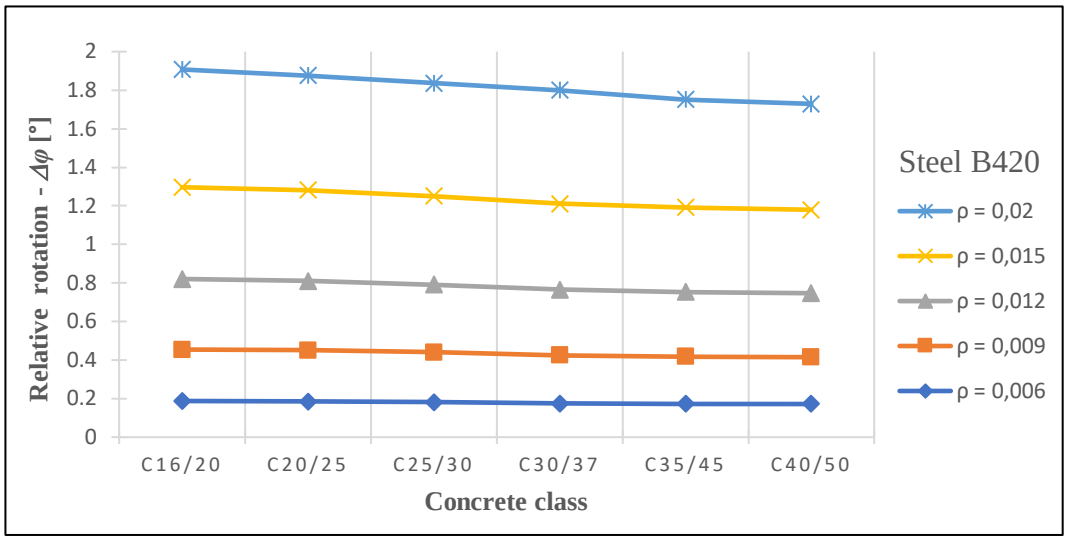

Figure 7. Relative rotation-concrete class for steel B420.

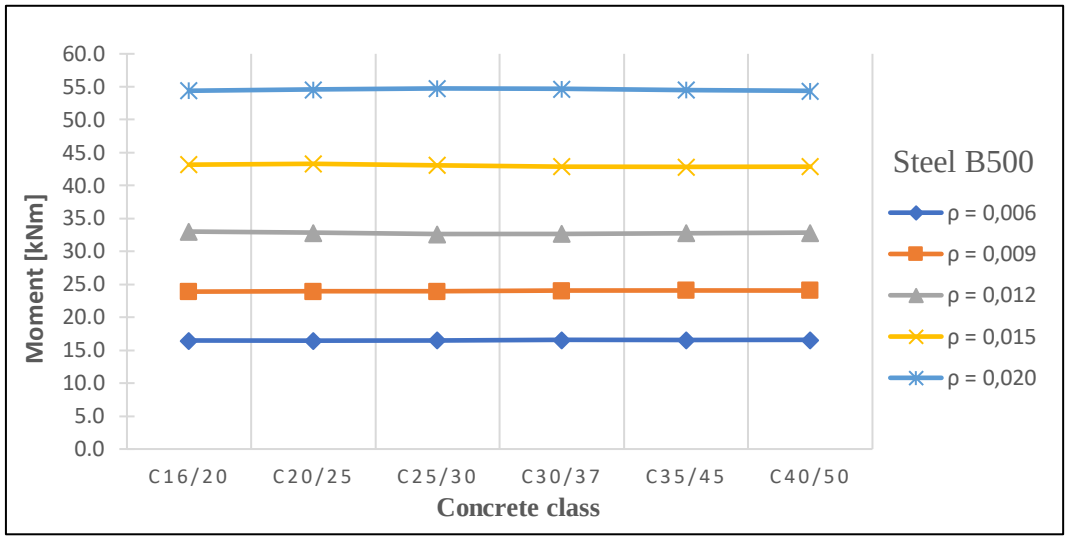

Figure 8. Bending moment-concrete class for steel B500.

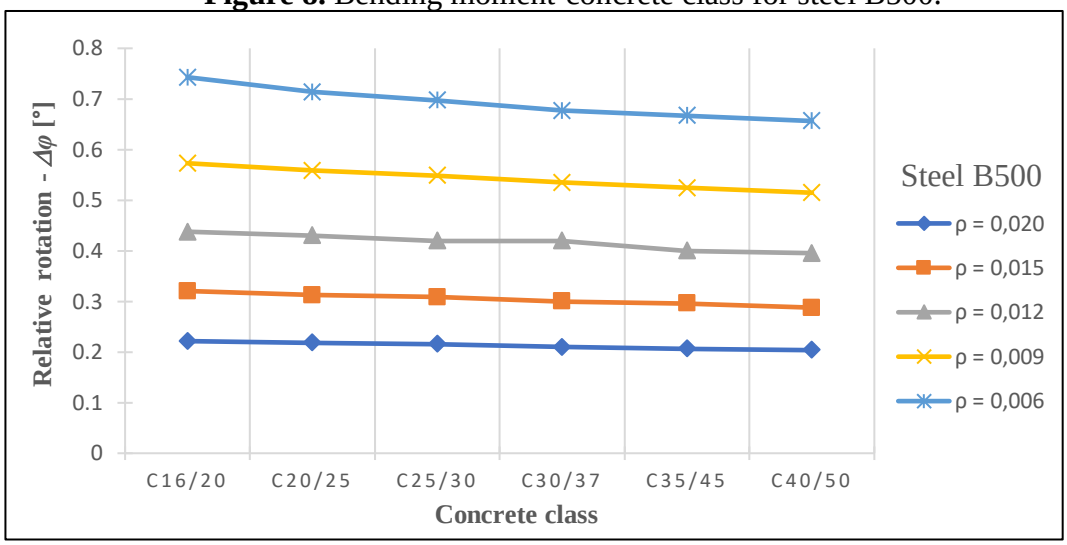

Figure 9. Relative rotation-concrete class for steel B500.

From the results presented in fig. 6 and 7, as well as from Table 2, it is evident that the moment predictably increases with the steel type and with the increasing of reinforcement ratio

too. On the other hand, the bending moment values practically do not change and do not depend on the concrete class. This result goes against expectations.

According to Eurocode [6] the height of the compressive zone is $\lambda.x$ and:

$$x = \frac{h}{2}, \tag{1}$$

for symmetrical cross section and λ = 0,8 for concrete with design strength $f_{cd} < 50\ MPa$. In (1) h is the height of the cross section.

Then for the bending moment in a reinforced concrete rectangular cross section:

$$M = \eta f_{cd} b \lambda x \left(d - \frac{\lambda x}{2}\right) \tag{2}$$

where ηf_{cd} is the design strength of concrete, η = 1 for concrete with design strength $f_{cd} < 50\ MPa$, b is the cross-section width and d is the effective height of the section.

According to expression (2), such an influence exists, and the bending moment depends on the strength of the concrete. Its value is expected to increase as the concrete class increases.

From fig. 8 and fig. 9, as well as from table 2, it can be seen that the relative rotation predictably decreases with increasing steel type and reinforcement ratio, while with respect to the concrete class remains almost constant. Regarding rotation, its value is expected to decrease with increasing concrete class, since a higher concrete class implies lesser deformability of the elements.

3. CONCLUDING REMARKS

In order to confirm the results presented here, further research is needed. One such study is to carry out a similar parametric analysis using another numerical model involving crack development and fracture mechanics parameters. On the other hand, it is necessary to do additional research by considering the concrete plasticity in the compression zone.

ACKNOWLEDGEMENT

Funding for this project and the research described herein was supplied by the National Science Fund under the contract № ВН – 275/23. Their support is gratefully acknowledged.

REFERENCES

[1] Hillerborg, A., Modeer, M. and Petersson, P. E.: Analysis of Crack Formation and Crack Growth by Means of Fracture Mechanics and Finite Elements. Magazine of Concrete Research, Vol. 6, pp 773 – 782, (1976)

[2] Smarzewski, P; Słowik, M. Numerical Analysis of Cracking Processes in RC Beams without Transverse Reinforcement. Processes 2023, 11, 584. https://doi.org/10.3390/pr11020584

[3] Kerelezova, I., Numerical modelling of quasibrittle materials by fracture mechanics approach, PhD thesis, UACEG, Sofia, 2002. (in Bulgarian)

[4] S. Parvanova, K. Kazakov, I. Kerelezova, G. Gospodinov, M. P. Nielsen, On a diagonal numerical crack model of RC beam with no shear reinforcement, Proc. of 10th Jubilee National Congress on Theoretical and Applied Mechanics, 13-16 September 2005, Varna, Bulgaria. (paper in proceedings)

[5] Ansys® Academic Research Mechanical, Release 18.1, Help System, Coupled Field Analysis Guide, ANSYS, Inc.

[6] EN 1992-1-1 Eurocode 2: Design of Concrete Structures—Part I: General Rules and Rules for Buildings. European Committee for Standardization, 2002.